Journal of Iron and Steel Research, International 24 (2017) 1065－1072

Contents lists available at ScienceDirect

Journal of Iron and Steel Research, International

journal homepage: www.chinamet.cn

Erosion corrosion of low-alloy wear-resistant steels in alkaline slurry

Feng-ming Song, Lin-xiu Du*

State Key Laboratory of Rolling Technology and Automation, Northeastern University, Shenyang 110004, Liaoning, China

ARTICLE INFO

Key words:
Erosion
Corrosion
Slurry
Synergy
Steel

ABSTRACT

Erosion corrosion causes significant problems in various industrial environments through a synergistic effect which results in much greater weight loss than the sum of the weight losses in the individual processes. The erosion-corrosion behavior of three low-alloy steels was investigated in a simulated concrete slurry using the rotation method. The key influencing factors and mechanism of material degradation were analyzed. The experimental results indicate that the weight loss increases with the linear velocity according to a nearly exponential relationship ($W=KV^n$), where n is 1.40－2.14. This weight loss is mainly caused by erosion in the alkaline slurry, and steels with higher tensile strengths show higher erosion-corrosion resistance. The formation of many platelets and ring cracks and their removal from the sample surface during erosion corrosion in the slurry are thought to constitute the mechanism responsible for this weight loss. These platelets and ring cracks are formed by solid particles striking the sample surface. Craters are initially produced and subsequently disappear as they grow and come in contact with each other. Fewer craters were observed on the surfaces of samples that exhibited higher weight loss. The surface of the material became work-hardened because of the effect of the particles striking and scratching, and a deformed layer was produced on the surface for steels of lower strengths, leading to deeper and more abundant gouges.

1. Introduction

Erosion corrosion commonly occurs in mining machinery plants, hydroturbines and delivery systems for liquid-solid particle slurries, such as ore, sand, and coal. This process gives rise to significant problems affecting the performance, reliability and lifetime of devices and components. Erosion and corrosion involve many mechanical and chemical mechanisms, and the combined action of these mechanisms often results in significant mutual reinforcement. Because of its synergistic effect, erosion corrosion has been shown to generate much greater weight loss than the sum of the weight losses in the individual pure erosion and pure corrosion processes[1-6].

Researchers have qualitatively studied the interactions between erosion and corrosion in specific environments, revealing that the relative importance of erosion, corrosion and erosion-corrosion synergism depends on the specific electrolyte, alloy, and service conditions[7]. Ones described the influences of experimental parameters, such as the angle of attack, slurry speed, sand particle size and sand concentration, on slurry erosion in seawater sand slurries[8]. In coal slurry, the erosion mechanism was determined to be related to platelet formation, similar to that observed in the gas-solid particle stream erosion of ductile metals[9]. In an oil sand slurry, the material loss caused by solid particles was dominant, whereas the contribution from corrosion was slight[10].

In slurry transportation systems for flue gas desulphurization and chemical processing applications, the material loss that is attributable to corrosion factors has been found to increase with acidity, chloride concentration and temperature. By contrast, the particle size is the most influential factor affecting the erosion-corrosion rate of high-Cr cast iron alloys. Large particles are much more effective in removing both the corroded surface layer and fresh material[11].

Solid-liquid concrete slurries contain high concentrations of river sand and carpolite, and the particle size is approximately 10－20 mm. The devices and components involved in concrete slurry mixing and delivery in concrete mixing vehicles and pumping lines have been found to suffer significant damage from erosion corrosion. For example, the 4 mm-thick

* Corresponding author. Prof., Ph.D.; Tel.: +86 13482372269.
E-mail address: *dulx@ral.neu.edu.cn* (*L.X. Du*).

Received 24 October 2016; Received in revised form 17 March 2017; Accepted 30 March 2017
Available online 15 October 2017
1006-706X/Copyright©2017, The editorial office of Journal of Iron and Steel Research, International. Published by Elsevier Limited. All rights reserved.

impellers utilized in concrete mixing drums usually degrade within two years. However, few studies have investigated the erosion-corrosion characteristics of steels in an alkaline concrete slurry.

The erosion-corrosion behavior of three low-alloy steels in a simulated concrete slurry was investigated using a modified rotating tester, and the key influencing factors and mechanism of material degradation were analyzed.

2. Experimental

2.1. Tested materials

The compositions and mechanical properties of the tested steels are listed in Table 1. Steel 1 is a common carbon steel that is widely used in concrete mixing drums. Steel 2 is a type of wear-resistant steel used in concrete mixing vehicles. Steel 3 is a newly developed steel with higher strength. Flat samples with dimensions of 5 mm×20 mm×65 mm were cut from each steel plate.

Table 1
Compositions and mechanical properties of tested steels

Tested steel	Composition/wt. %				Mechanical properties				
	C	Si	Mn	Other	C_{cq}*	$R_{p0.2}$/MPa	R_m/MPa	A/%	Hardness/HV
1	0.16	0.22	1.49	—	0.418	452	609	27	184
2	0.14	0.30	1.63	0.05Nb－0.3Cr－0.1Mo	0.509	631	741	21	233
3	0.30	1.50	2.00	0.8Al	0.540	673	1250	12	365

Note: C_{cq}* =C+Mn/6+Mo/4+Cr/5+V/14+Si/24+Ni/40.

2.2. Experimental methods

The apparatus used for the erosion-corrosion tests consisted of a rotating disk with eight samples mounted symmetrically at the edge (Fig. 1). The slurry was prepared by adding 39.5 kg quartz to 14.0 kg tap water (74 wt. %); the diameter of the quartz particles was approximately 3 mm. The pH of the slurry was adjusted to 12.1 by adding NaOH.

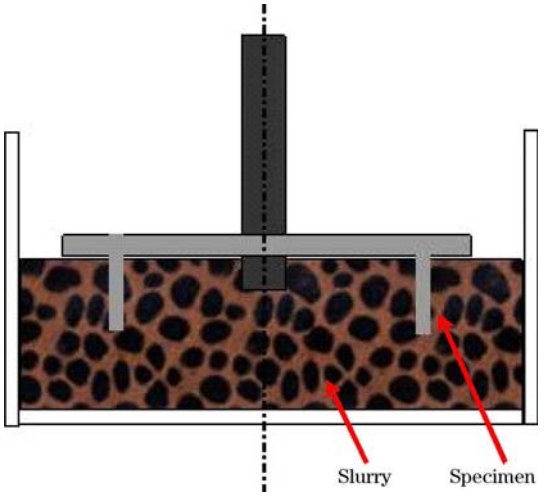

Fig. 1. Schematic diagram of rotating corrosion abrasion tester.

Rotational speeds of 50, 100 and 150 r/min were selected based on the typical running speed of a concrete mixing drum (approximately 2 m/s) and corresponded to approximately linear velocities V of 1.1, 2.2 and 3.3 m/s, respectively. The tested distance was 60 km, so the testing time was approximately 15, 7.5 and 5 h, respectively. The weight losses of the samples were determined by calculating the difference between the initial and final weights measured using a high-precision analytical balance with a sensitivity of 0.1 mg. Because of variations in the sample size, normalized erosion-corrosion rates were measured in terms of the weight loss per unit area (mg/cm^2). The temperature of the slurry at the end of the experiment was taken to be the testing temperature and was measured using a thermocouple. The surface morphologies of the specimens after the erosion-corrosion test were observed via scanning electron microscopy (SEM).

Generally, the total weight loss resulting from erosion corrosion (W_t) can be divided into the following components: the weight loss due to pure erosion (W_e), the weight loss due to pure corrosion (W_c) and the weight loss due to the synergistic erosion-corrosion effect (W_s)[10]. W_s can be calculated as follows:

$$W_s = W_t - W_c - W_e \quad (1)$$

Additional specimens were statically immersed in the slurry for the same duration as that of the erosion-corrosion test, and the difference in their weights before and after testing was defined as the weight loss due to pure corrosion. Moreover, a pure erosion test was conducted in a slurry of tap water and 74 wt. % silica particles at the same velocity as the erosion corrosion test; in this test, anodic protection was applied by means of a zinc bar mounted on the disk to suppress the corrosion process.

2.3. Experimental procedure

Two identical specimens of each type of steel were used in every test. The surface of each specimen was polished and dried after being cleaned with alcohol, and the specimen was then weighed before being

mounted to the disk using a screw. After testing, the specimens were cleaned in a 50 wt. % hydrochloric acid solution containing Aminoform to remove the rust from their surfaces. Then, the specimens were cleaned with alcohol, dried and weighed.

3. Results and Discussion

3.1. Microstructure

Steel 1 is a common carbon structural steel with a ferrite and pearlite microstructure, as shown in Fig. 2(a). Steel 2 is a wear-resistant steel that exhibits a granular bainite microstructure (Fig. 2(b)), whereas steel 3 was designed to have a higher C-Si-Mn composition. The results of a metallographic analysis showed that steel 3 contains approximately 15 vol. % ferrite (Fig. 2(c), white) and 6－8 vol. % retained austenite; the balance was determined to be martensite (Fig. 2(c), grey), with a large amount of precipitated carbides distributed throughout the lath martensite (Fig. 2(d)). The martensite endows this steel with high strength, and the ferrite provides excellent ductility. The retained austenite is expected to transform into martensite during cold deformation, thereby re-strengthening the steel. Therefore, steel 3 exhibits excellent wear resistance and workability.

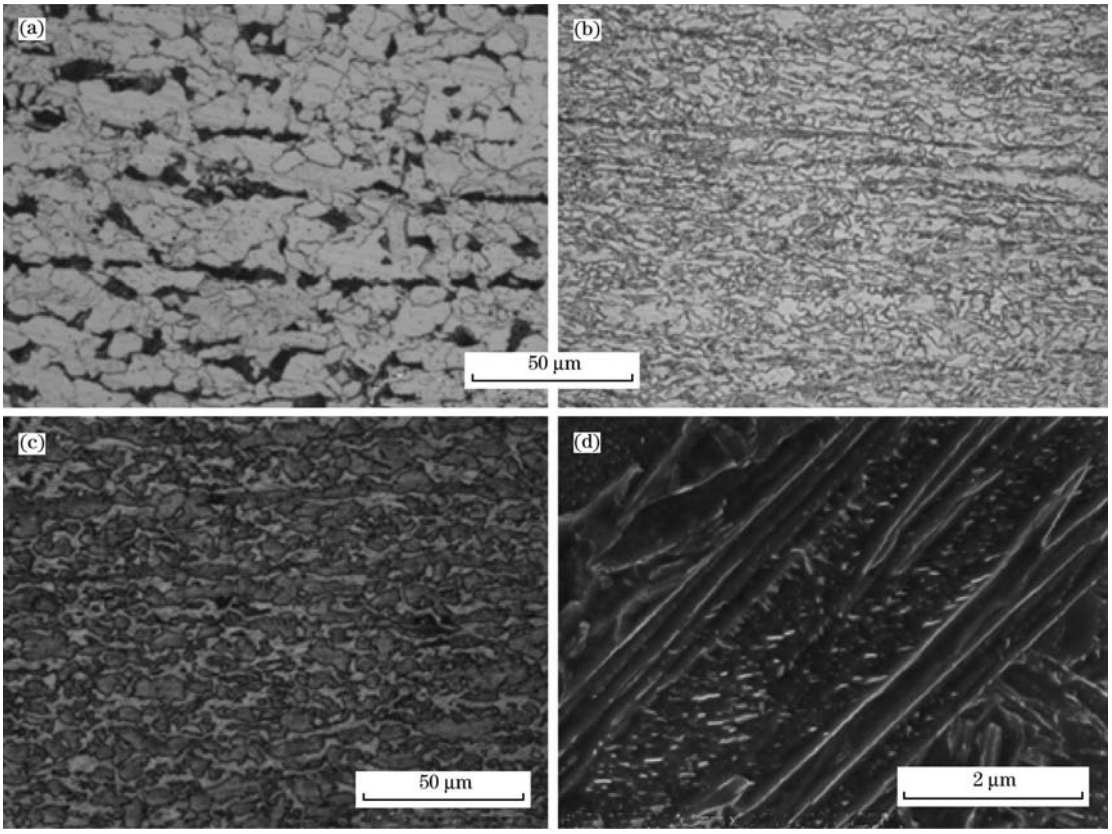

(a) Steel 1; (b) Steel 2; (c), (d) Steel 3.

Fig. 2. Microstructures of tested steels.

3.2. Effect of velocity

The weight losses of the specimens due to pure corrosion, pure erosion and the synergistic erosion-corrosion effect are reported in Table 2 and Fig. 3. The experimental results show that the weight loss per unit area increased rapidly as the test velocity increased (Fig. 3) and that the weight loss caused by pure corrosion represented only a small percentage of the total weight loss, indicating that erosion was

Table 2
Weight loss values for tested steels

V/(m·s^{-1})	Time/h	W_t/(mg·cm^{-2})			W_c/(mg·cm^{-2})			W_c/(mg·cm^{-2})			W_s/(mg·cm^{-2})		
		1	2	3	1	2	3	1	2	3	1	2	3
1.1	15.0	5.43	4.36	2.54	0.52	0.46	0.48	4.68	3.70	1.86	0.24	0.20	0.20
2.2	7.5	15.47	13.14	6.68	0.22	0.18	0.23	10.34	9.56	4.98	4.92	3.40	1.47
3.3	5.0	51.70	45.22	26.57	0.15	0.10	0.11	49.80	43.31	25.36	1.75	1.81	1.09

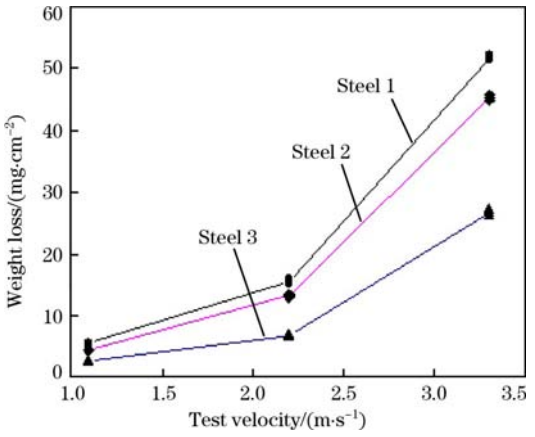

Fig. 3. Weight loss values of tested steels determined at different test velocities.

the primary contributor.

The slurry erosion phenomenon is not yet fully understood because of the complex synergy that exists between the erosion and corrosion processes. An earlier study of erosion predicted that the volume of material removed should depend on the particle velocity: volume=(velocity)^n, where the value of n is variable[12]. Aso et al.[13] investigated the slurry erosion behavior of Fe-Cr-C-B eutectic alloys and found that the rate of erosion corrosion increased exponentially as the fluid velocity increased:

$$W = KV^n \quad (2)$$

where, W is the weight loss per unit area; K is a constant; and n is the value of the exponent. The value of the exponent n varied with the particle velocity, particle concentration and material properties, and for metals, it was typically between 2 and 3.

The experimental results reported here showed a similar trend (Table 3), with the value of n increasing with increasing velocity. When the linear velocity changed from 2.2 to 3.3 m/s, n increased from 1.40－1.59 to 2.05－2.14. However, no clearly defined value could be assigned to the n exponent, possibly because of the difference in the mechanism of attack due to the simultaneous and synergistic interaction between erosion and corrosion.

Table 3
Values of erosion-corrosion velocity exponent n

V/(m·s^{-1})	Steel 1	Steel 2	Steel 3
2.2	1.51	1.59	1.40
3.3	2.05	2.13	2.14

For the comparison of the different steels, a comparative erosion-corrosion weight-loss ratio was defined as the erosion-corrosion weight loss of one of the tested steels (2 or 3) divided by the erosion-corrosion weight loss of steel 1, which was treated as the reference steel. Fig. 4 presents the comparative weight-loss ratios of steels 2 and 3. The comparative weight-loss ratios of both types of specimens showed a slight tendency to rise with increasing velocity, although that of steel 3 actually decreased slightly at 2.2 m/s. The weight loss caused by corrosion markedly decreased at 2.2 m/s, especially for steel 3 (Table 2); this behavior could be related to the test temperature. In general, the rate of corrosion tended to increase as the temperature increased. However, the temperature was lower at 2.2 m/s, which caused the corrosion rate to decrease. This finding indicates that the influence of corrosion significantly enhanced the erosion-corrosion weight loss. Therefore, the erosion-corrosion weight loss decreased at lower temperatures, as reflected by the corresponding slight decrease in the comparative weight-loss ratio.

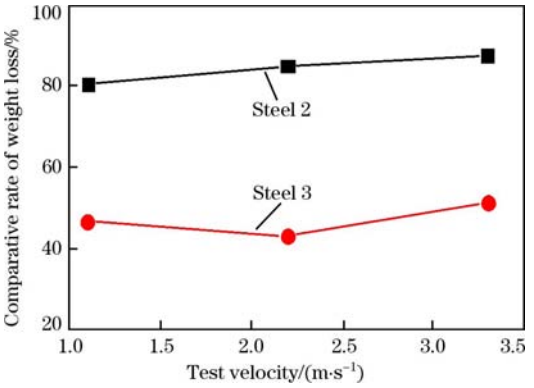

Fig. 4. Comparative weight-loss ratios of tested steels 2 and 3 compared with reference steel 1.

The comparative weight-loss ratio of steel 3 was small, approximately 43%－51%, indicating that its erosion-corrosion resistance was nearly twice as great as that of steel 1. By contrast, the comparative weight-loss ratio of steel 2 was 80%－87%, indicating that its resistance to erosion corrosion was similar to that of steel 1, which is consistent with experience from practical applications. The resistance to erosion corrosion exhibited a nearly linear relationship with the tensile strength, implying that the steel with a higher strength is better able to resist erosion corrosion in an alkaline slurry.

3.3. Effect of composition

Both erosion and corrosion contribute to the weight loss caused by erosion corrosion[10], and increasing resistance to corrosion and wear is an effective means of improving resistance to erosion corrosion. Table 4 shows the percentage contributions of pure corrosion, pure erosion and erosion-corrosion synergy to the total erosion-corrosion weight loss.

The percentage contribution of pure corrosion in all

Table 4
Components of erosion-corrosion weight loss

V/(m·s^{-1})	W_c/%			W_c/%			W_s/%		
	1	2	3	1	2	3	1	2	3
1.1	9.51	10.50	19.03	86.13	84.94	73.12	4.36	4.56	7.85
2.2	1.40	1.33	3.50	66.83	72.79	74.50	31.77	25.88	22.00
3.3	0.28	0.22	0.43	96.33	95.77	95.46	3.39	4.01	4.11

steels decreased rapidly as the velocity increased because the weight loss induced by erosion increased. Compared with steels 1 and 2, the corrosion weight loss contributed to a higher percentage of the total weight loss in steel 3 because of its higher carbon content (Table 1). Carbon present in steel can transform into carbide and act as a cathode because of its higher potential, thereby accelerating the corrosion rate and leading to more erosion-corrosion weight loss[14]. Therefore, the percentage of weight loss caused by corrosion in steel 3 was relatively high.

Two reasons can explain the reduction in the fraction of the weight loss caused by pure corrosion as the velocity increases: First, the striking and microcutting effects of solid particles on the surface are stronger at higher velocities, which caused the weight loss caused by erosion to increase rapidly; Second, the corrosion time decreased as the test velocity increased. The combined impact of these two effects led to the observed variation in the corrosive contribution.

Pure erosion was responsible for the largest fraction of the total degradation in the slurry erosion-corrosion experiment, as shown in Table 4. Whereas the corrosion component was only 1.33%－3.50% of the total weight loss, and the weight loss resulting from erosion-corrosion synergy was significant, representing 22.00%－31.77% of the total degradation (2.2 m/s). This finding is in good agreement with the results of Watson[7].

The synergy between erosion and corrosion plays an important role in the material removal process[15], often significantly increasing material degradation. The magnified synergistic effect may be attributed to surface roughening and the removal of the hard phases by corrosion. Indeed, corrosion products can also cause erosion. Noel and Ball[16] found that the formation of a hardened layer is impeded by corrosion. Although the effect of erosion on corrosion has been determined to be related to the recovery rate of passive films broken by scratching, and the thermodynamic stability of steels is decreased by friction[17], erosion shifts the corrosion potential in the more active direction, and the corrosion current density increases by approximately two orders of magnitude[15].

Although the weight loss fraction of pure corrosion of the total weight loss among the three tested steels was the highest at 1.1 m/s, the synergy of corrosion and erosion was much lower. The corrosion time clearly increased as the test velocity decreased at the same erosion distance, but the corrosion velocity remained constant, which explain the reduction in the fraction of the weight loss caused by synergy at 1.1 m/s. The synergy of corrosion and erosion decreased rapidly as the rotation velocity increased to 3.3 m/s. The reason for the decrease in synergy at 3.3 m/s is the short corrosion time and the drastic erosion caused by the higher test velocity. The mechanism of the synergistic effect between corrosion and erosion is complicated, and further investigation is needed.

The results presented in Table 4 show that the synergy decreased as the steel strength increased (2.2 m/s), indicating that the enhancement of erosion by corrosion also decreased, leading to improved erosion-corrosion resistance. Although the corrosion resistance can be improved by the formation of a protective rust layer, this mechanism did not occur in the erosion-corrosion environment examined here. Therefore, the corrosion weight loss of steel 3 was higher than that of steels 1 and 2.

3.4. Morphology resulting from erosion corrosion

Micrographs of the erosion-corroded surfaces were obtained via SEM. The surface usually exhibited large numbers of scratches, gouges and holes or craters resulting from the combined effects of corrosion and erosion[18]. Small numbers of craters were observed on the surfaces of steels 1 and 2 (Fig. 5), which showed higher weight loss, whereas more abundant craters were observed on the surface of steel 3. This was especially true in the upper regions (Fig. 5(d)), where the erosion corrosion was less significant. The crater diameter was approximately 50－150 μm. The surfaces subjected to the highest test velocity were not as smooth as those tested at 1.1 m/s (Fig. 6), showing the formation of additional gouges.

The appearance of the craters on the surfaces described here suggests that craters were produced during the initial stage and that the number and diameters of the craters increased during the test until they came into contact with one another. Subsequently, the craters disappeared, and uniform erosion corrosion occurred.

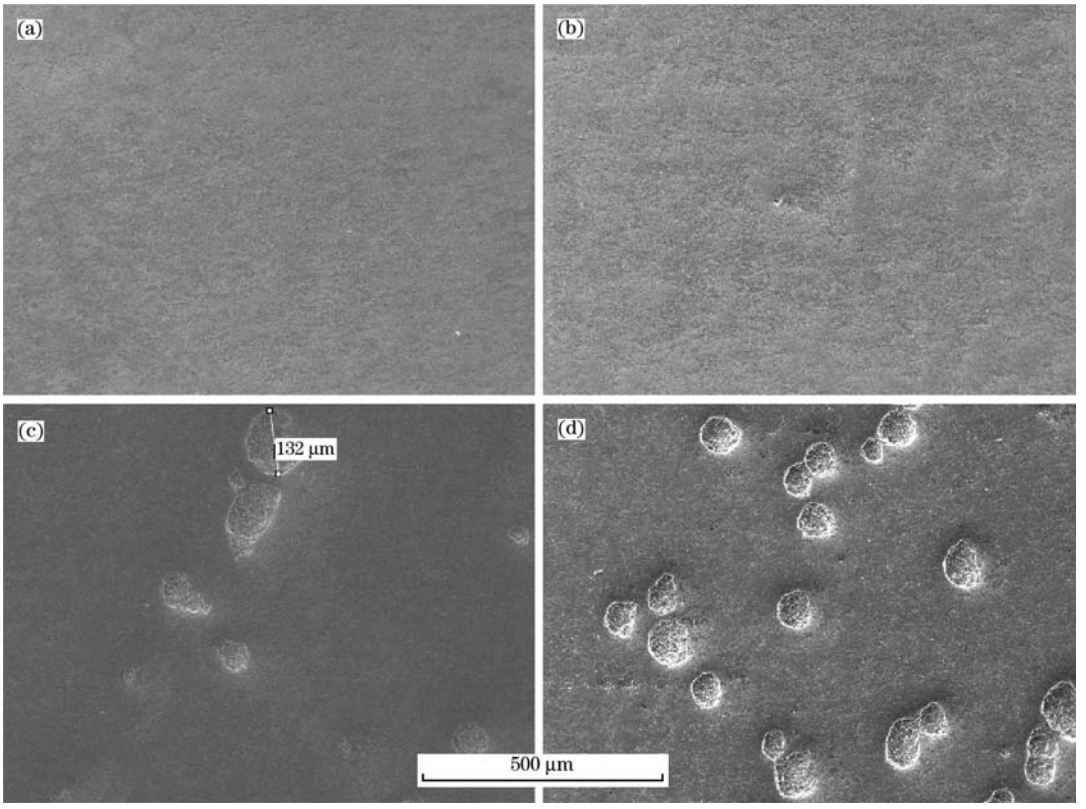

(a) Steel 1; (b) Steel 2; (c) Steel 3; (d) Upper region of Steel 3.

Fig. 5. SEM micrographs of erosion-corrosion surfaces (1.1 m/s).

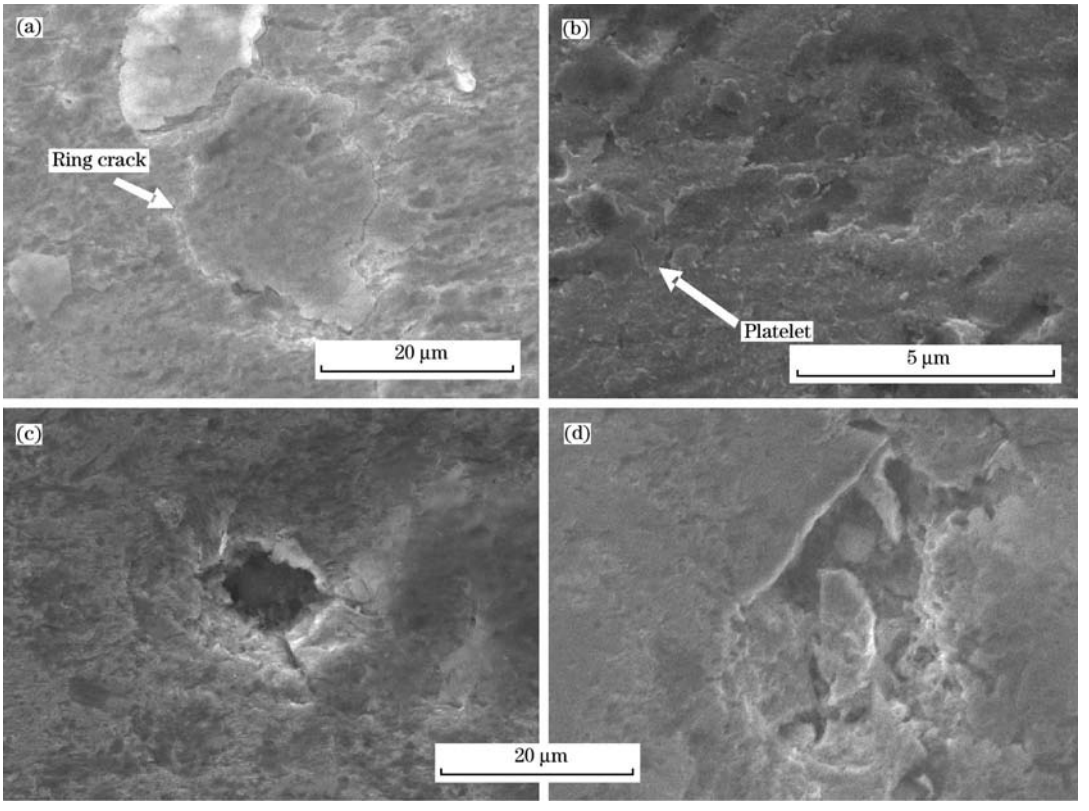

(a) Steel 1; (b) Steel 3; (c) Steel 2; (d) Steel 3.

Fig. 6. Micrographs showing surfaces in detail (1.1 m/s).

Voloshyn and Kosarevych[19] studied the initial stage of the erosion-corrosion destruction of thermally treated steel in alkaline environments with pH values of 13.4 to 13.7 and found that the initial craters had diameters of approximately 10 μm and were randomly distributed on the surface. With the striking of subsequent particles, the craters gradually grew until many craters began to come in contact with each other. Specifically, small craters (10 μm in diameter) formed during the first several seconds and subsequently increased in size to approximately 150 μm over time. These results reveal why more craters were not observed on the surfaces of steels 1 and 2: as the weight loss increased, the number of craters decreased.

The details of the craters and the erosion-corrosion surfaces were observed at a high magnification, and many ring cracks and platelets that were evident were later removed (Fig. 6). These platelets were presumably removed relatively easily by the striking and microcutting action of particles[20], which was considered by Noelmar to be the main mechanism of material removal[21].

Typically, the strain that occurs during erosion is very large[3], and the surface becomes work-hardened by the eroding particles. Because of the striking of subsequent particles at sufficient impact velocities, ring cracks (Fig. 6(a, b)) appeared near the contact area. These ring cracks propagated deeply and formed a frustum of cones. The number of concentric ring cracks increased as striking increased. The volume removed by the impacting particles was assumed to be proportional to the volume bounded by the outermost ring crack and the depth of the initial ring crack prior to crater formation (Fig. 6(c, d)). Features resembling steps could be seen at the edges of the newly formed craters.

The erosion-corrosion surface became increasingly rough at higher velocities (Fig. 7). The kinetic energy of solid particles increases with increasing the velocity, and gouging occurred when the particles struck the surface. Some particles fractured after impacting the surface, and the tips of these particles dug deeply in the soft surfaces of the specimens (Fig. 7(a)). This gouging process was more difficult in steel 3 because of its higher strength and hardness. As a result, the gouges were shallower and did not form as frequently.

Fig. 8 presents cross-sectional images of the surfaces of steels 2 and 3. A deformed layer on the surface can be clearly seen (indicated by the arrow in Fig. 8) in the steel 2 specimen. By contrast, on the surface of the steel 3 specimen, platelets that could be easily removed are present, but no deformed layer is observed. Aribo et al.[22] revealed that under sand impingement, the sub-surface becomes work-hardened.

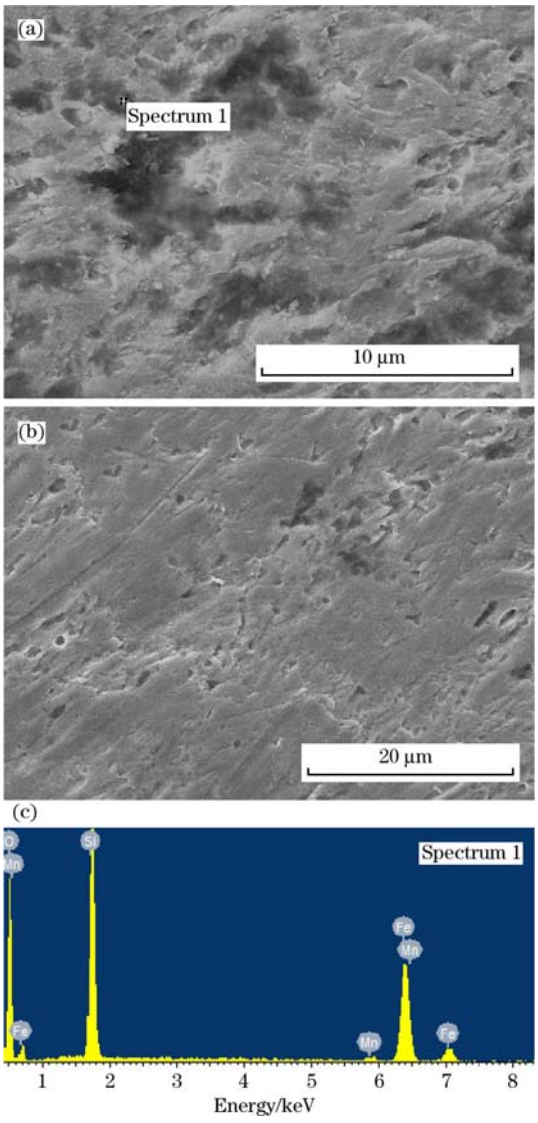

(a) Steel 2; (b) Steel 3; (c) Composition of spectrum 1.

Fig. 7. Micrographs of erosion-corrosion surfaces (3.3 m/s).

Thus, a deformed layer forms on the work-hardened surface of a material, which tends to be cracked by subsequently striking particles, leading to the appearance of craters and enhancing the removal of material.

4. Conclusions

(1) The erosion-corrosion weight loss per unit area increased rapidly as the test velocity increased; the weight loss and velocity exhibited an exponential relationship ($W = KV^n$), and the value of n increased as the velocity increased.

(2) The weight loss caused by erosion by solid particles was dominant in the concrete alkaline slurry at 2.2 m/s, whereas the contribution from corrosion was slight; nevertheless, corrosion clearly enhanced the erosion-corrosion weight loss. The synergistic erosion-corrosion effect was significant, repre-

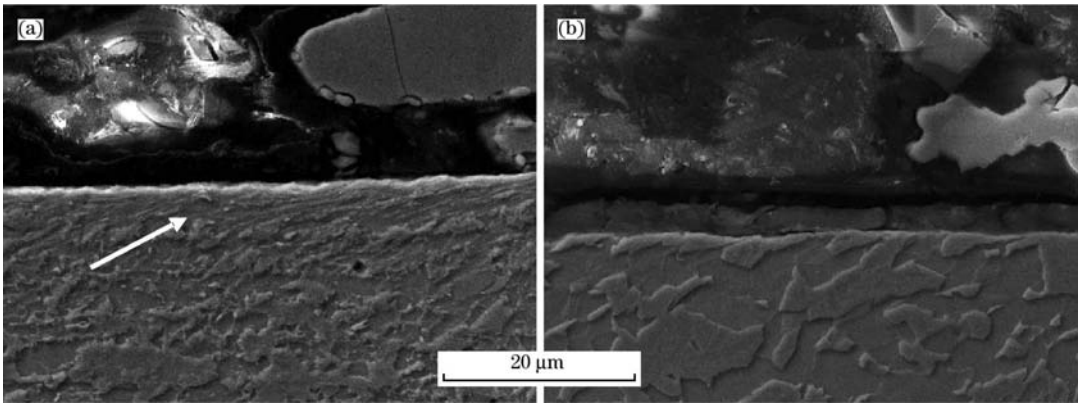

(a) Steel 2; (b) Steel 3.

Fig. 8. Cross-sectional images of specimens showing presence of a deformed layer and platelets.

senting 24%—36% of the total degradation.

(3) Steels of higher strength showed improved erosion-corrosion resistance in the alkaline slurry, whereas the formation of a protective rust layer did not show a similar effect. The erosion-corrosion resistance of steel 3 was twice that of steel 1, and that of steel 2 was 80%—87% that of steel 1, consistent with experience from practical applications of these materials.

(4) Craters were produced during the initial stage of degradation, and the number and diameters of the craters increased during the test until the craters came in contact with each other. Subsequently, the craters disappeared, and uniform erosion corrosion occurred. Fewer craters were observed as the weight loss increased.

(5) The formation and removal of platelets and ring cracks was determined to be the main mechanism underlying erosion-corrosion weight loss in an alkaline slurry. The surface of the material became work-hardened, and ring cracks formed because of the striking of particles. Subsequently, uniform erosion corrosion occurred as more craters came in contact with each other. The effect of the particles striking and scratching the surface was enhanced at higher velocities, and a deformed layer was produced on the surface for steels with lower strengths, leading to deeper and more abundant gouges.

References

[1] Z. Karl-Heinz, D. V. Doane, Metall. Trans. A 11 (1980) 613-620.
[2] Y. Zheng, Z. Yao, X. Wei, W. Ke, Wear 186-187 (1995) 555-561.
[3] I. Finnie, Wear 186-187 (1995) 1-10.
[4] I. Finnie, J. Finnie, J. Mater. 2 (1967) 682-700.
[5] R. Baker, N. Bessaih, Proc. Inst. Civ. Eng. Water, Marit. Energ. 118 (1996) 199-203.
[6] D. K. Goyal, H. Singh, H. Kumar, J. Eng. Tribol. 225 (2011) 1092-1105.
[7] S. W. Watson, F. J. Friedersdorf, B. W. Madsen, S. D. Cramer, Wear 181-183 (1995) 476-484.
[8] J. W. M. Mens, A. W. J. de Gee, Tribol. Int. 19 (1986) 59-64.
[9] A. V. Levy, N. Jee, P. Yau, Wear 117 (1987) 115-127.
[10] Y. C. Yang, Y. F. Chen, Wear 276-277 (2012) 141-148.
[11] H. H. Tian, G. R. Addie, R. J. Visintainer, Wear 267 (2009) 2039-2047.
[12] I. Finnie, D. H. McFadden, Wear 48 (1978) 181-190.
[13] S. Aso, S. Goto, Y. Komatsu, J. Jpn. Inst. Met. 62 (1998) 774-782.
[14] S. Z. Li, X. Jiang, Corros. Sci. Protect. Technol. 7 (1995) 122-129.
[15] Z. Y. Yue, P. A. Zhou. J. Tribol. 7 (1987) 65-72.
[16] R. E. J. Noel, A. Ball, Wear 87 (1983) 351-361.
[17] J. Heidemeyer, Wear 66 (1981) 379-387.
[18] M. C. Park, K. N. Kim, G. S. Shin, S. J. Kim, Wear 274-275 (2012) 28-33.
[19] V. A. Voloshyn, R. Y. Kosarevych, Mater. Sci. 49 (2013) 398-403.
[20] A. V. Levy, G. Hickey, Wear 117 (1987) 129-146.
[21] N. P. Abbade, S. J. Crnkovic, Tribol. Int. 33 (2000) 811-816.
[22] S. Aribo, R. Barker, X. Hu, A. Neville, Wear 302 (2013) 1602-1608.